Boundary conditions and Natural temperature decay from experimental data analysis to on-design of a tank for CSP plant Part 1

Alfredo Angelillo[1], Walter Gaggioli[2] and Primo Di Ascenzi[2]

1 REEFs–Dfind AS, Oslo (Norway)

2 ENEA–Italian National Agency for New Technologies, Energy and Sustainable Economic Development, Rome (Italy)

Abstract

Applying the real boundary conditions and the time differential in a thermal volume implies the possibility of modeling the heat transfer dynamically, in this case determining an inertial accumulation of thermal energy of any kind. Hence, the ability to control heat losses and know the temperature trend of a tank on the walls can provide an interesting and innovative tool to guide solutions regarding the design of a molten salts Thermal Energy Storage (TES). The paper objective is first to have solved equations during a natural decay of temperature, for extending the following parts the discharging phases to most efficient design solutions. From the data of the experimental campaigns conducted since 2004, a thermodynamic solution has been modelled based on lumped-circuit abstraction under a set of imposed assumptions in a novelty way. This has been analyzed through a molten salt tank at experimental concentration solar power plant of Research Centre ENEA in Rome. Specifically, this Part 1 presents the method in use, namely that of simulating in a new way the value of the initial energy of a system different from zero as a function of the variation of time starting from a classical formula of the heat transport equation and using a lumped-circuit abstraction that can be better suited to variations and to the impositions of the boundary conditions. As a result, this paper holds the evidence between another use of lumped-circuit abstraction with no-zero initial energy varying on time as best modelling of real boundary conditions and a matching with known fundamentals in transient conduction, at the first time. That has been observed in a numerous natural discharging phases according to analyzed data (Appendix A). The result contributes to a greater understanding of heat transport and therefore to better orient the design choice. Finally, it has recalled the ongoing further developments of such new full-bodied modelling because such model based on the real conditions in use has different results according to an abstract switch witch open/close circuits depending on the variation of a component in function (Fig. 3).

Keywords: Lumped-circuit, Thermodynamic, Solar energy, Tank-storage

1. Introduction

The analysis during the experimental campaigns at ENEA Casaccia since 2004, and the last two ones with programme SFERA III 2020-21, show that the trend of the internal temperatures of a thermocline can be studied from the external thermocouples, in accordance with the relative cataloguing of data. Even though heat losses don't seem to have any occurrences or consequences through the tanks along the energy production, those have a significant role in the trend of extraction at right temperature, especially for thermocline. As first step, the study holds how the heat losses in a tank affect the internal temperatures without simplifications but setting boundary conditions close to a matter of facts. Therefore, the settings start from the data of the experimental campaigns to a modelled solution based on lumped-circuit abstraction under a set of imposed assumptions. The final purpose by observing the natural decay of temperatures as well as the level of molten salts, and stored energy is to optimize further the design and Distributed Control System during the discharging phase. Trivially, two conditions can be summarily identified, those in the discharge phase of the accumulated energy and those of heat losses in the charging phase, in the absence of significant atmospheric conditions, ceteris paribus.

On the condition that the focus is about the discharging phase, the points where there are heat losses must be identified and quantified consistently with the tank geometry and shapes. The Fig. 1 exemplifies how has been identified the areas of tank where the energy is lost direct to free stream conditions as specified further. Similarly, this has be done for all the point of tank. Those points according to temperature trend explain some

doi:10.18086/swc.2021.33.01 Available at http://proceedings.ises.org

crossing over between the curves when they are going to be observed closer. Besides, the boundary conditions of the thermocline have generally been limited to adiabatic conditions and omission of the perimeter bands to the tank. As result, the mathematical model applied to the system in operation and not simulated one imply a mismatch between an existing internal convection and radial motions and the temperature demand, namely lowering ability to extract a right flow temperature and its operating performance. In other word, it is not pointless to study the heat flow from inside to outside in operating mode to promote improvement and orientation for new storage solutions.

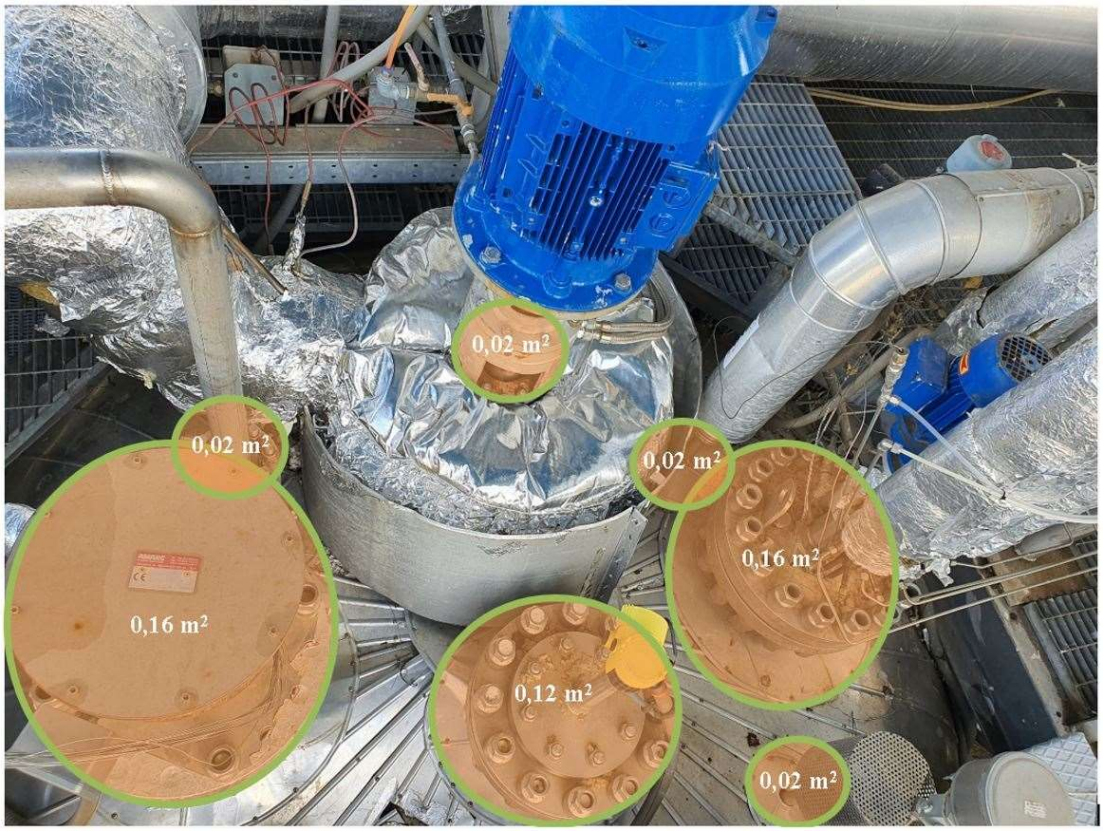

Fig. 1 Identified heat loss points on the top of molten salt tank SA.1.01

As matter of fact according to historical data, each operating day at experimental plant in Rome was recorded with date, hour when activity took place, eventually comments and especially values set in operation since 2004. For instance, the Fig. 2 shows what happened along a day. Peculiarly, it is known, according to the Fig. 2, that CS.1.01 was ON at 11 o'clock as well when the pump inside the tank was ON at 14:45 and OFF at 15:00 because of air-heater obstruction. Accordingly, when, and how long the reached temperatures at several blocks were known as well as the percentage of required power. Indeed, the initial and final temperatures along a planned process were known. As a result of this, to talk about real boundary conditions means use of real procedure in progress and known value where no doubt can be arisen. Matching the data with occurred activities on the plan, has permitted to outline the temperature on the tank-skin with a different point of view. Hence, the heat losses have had another significance values regarding the inside tank and motion or not of molten salt volume inside. Of course, this paper is limited to find out a specific equation which can correctly represent the temperature trend without other important boundary conditions. For instance, the dashed simulated green line in Fig. 2 shows the perfect matching of initial temperature (first green circle on the left side of curve) and the final lowered temperature (second green circle on the right side of curve).

Finally, the fundamentals of heat and mass transfer in relation to the principles of electrostatics, and more generally for what concerns inductances, resistances and capacities intended also in AC for some configuration, has been used to aid the right modelling of equations. Although this sensitive part will be dealt in a depth subsequent work, it is worth mentioning the conditions of natural temperature decay correspond to electrostatics conditions. This is going to introduce in the present paper to explain the nature of logic for such

novel type of lumped circuit abstraction (see Fig. 3) being applied with time-dependent initial energy for heat transfer.

Naturally, such association between the forms of heat transport, both steady-state and thermal transients, are not new in the field, but here the logic finds a new application. On that account, the idea to develop such full-bodied method can also be achieved thanks to the available automation technology when the concept of having multi-switch conditions (see Fig. 3) are activated according to the existing boundary conditions.

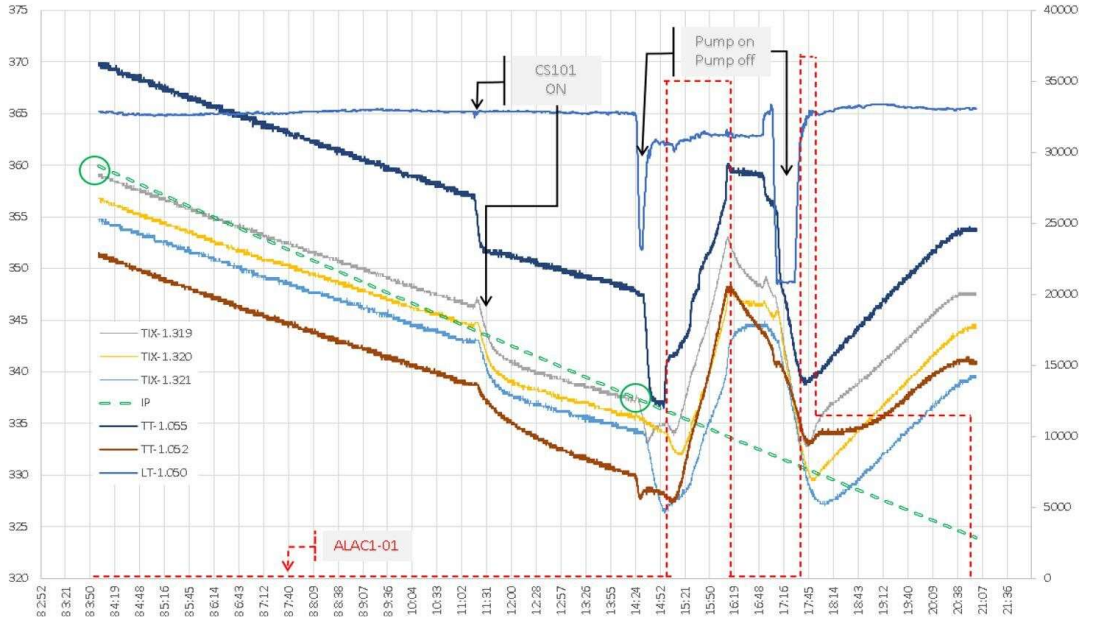

Fig. 2 Typical day compared to Experimental Plant Log Record where components' switching on/off can observed accordingly. TIX-1-3NN are thermocouples on the tank-skin. TT-1-05N are thermocouples installed at 100 mm from the tank-skin. LT-1-050 is the measured level of molten salt into the tank. The red dashed line ALAC1-01 is the electrical power supplied to the tank when switched on [Watt on the right y-axe]. The dashed green line named IP is the simulated one according to the boundary conditions defined between the two points (green circles). Left Y-axe are temperature while X-axe is time along the experimental day in 2008.

2. Method

Since previous papers (Garimella, Flueckiger, 2012; Chao Xu et al. 2012; Gaggioli et al., 2018), particularly Preliminary Design Study in 2010 (Turchi et al. 2010), about simulated charge and discharging conditions validated on experimental data (Pacheco, Showalter, Kolb, 2002), a perimeter band thickness near the thermocline walls showed an involved area by a convectional motion, also mentioned in Zavoico, 2001. Concerned and assumed the same form factor, this perimeter thickness can statistically be calculated:

$$t_{conv} = 0{,}05 * \emptyset_{i,tank} \quad \Leftrightarrow \quad \frac{H}{\emptyset_{i,tank}+2t_0} = 1{,}0962 \qquad \text{(eq.1)}$$

The thermodynamic parameters of materials were found in the literature (Zavoico, 2001; Green, Perry, 2008; Bergman, Lavine, 2017) as function of temperature between 260 to 600°C and compared with the values of the technical data sheets of the products in use. The geometric values of the tank and its layers were respectively approximated as following:

- the thicknesses of the materials **t** in geometric averages.
- the linearized development of curves measured in AutoCAD® in rotation surfaces.
- the surfaces measured in AutoCAD® of the actual shapes in rotation volumes.

Since the heat loss of the curved surfaces of the tank is less than an angle of ± 30° from the horizontal plane, they have been simplified into vertical and horizontal ones – considering the heat transport on this curved surface underlies an insignificant residual volume (EN ISO 6946: 2017) –. The actual comparison between real shape/volume and simplified one is approximately 0.1%. Practically, no simplification or rounding is

performed on the real quantities of the tank and its form factors, even though the simulated shape has been based on an equivalent cylinder.

The time periods, where this study is based on, cover observations during the years 2004, 2008, 2018 and the last two experimental campaigns of SFERA III 2020 and 2021 as summarized in Appendix A. The most of initial data come since 2004 which are fundamental because of beginning of experimental solar power plant at ENEA in Rome. All these experimental data, received and analysed, have been compared with operating values and log registration to estimate the boundary conditions accordingly. Therefore, from the observation of the data and the application of a simple natural regression of these, it was verified whether the value of a hypothetical coefficient was factual, and if it could have been expressed as dependent on physical parameters, not exclusively as a mathematical one. Therefore, as a first approximation, an average value was evaluated from the regressions obtainable with respect to the temperatures recorded by the thermocouples assuming that data named b:

$$b = \left(\prod_i b_i\right)^{1/i} \quad \text{(eq.2)}$$

This made it possible to compare a single value in relation to a single thermocouple and therefore trivially with respect to each coefficient. It was mathematically obtained that:

$$a = \frac{y_i}{e^{-b\tau_i}} \; ; b = -\frac{\ln\left(\frac{y_i}{a}\right)}{x_i} \quad \text{(eq.3)}$$

The mathematical solution, according to the assumptions made in the introduction, must involve the physical one, that is:

$$b \propto f\left(\frac{h_c A}{\rho V c_p}\right) = f\left(\frac{h_c}{\rho c_p}\left(\frac{A}{V}\right)\right) \quad \text{(eq.4)}$$

Where it is observed that the ratio (A/V) is a shape ratio and therefore dependent on the geometry of a tank, thermocline, or storage. The other factors are physical parameters of which the density and specific heat can be considered constant as first stage in the given known range of temperatures. Besides, the convection coefficient h_c varies according to the interface and the type of occurred convective motion, assumed there is no mass exchange between the layer interfaces at first stage of analysis. The physical parameters of reference are strictly dependent on the materials, and, on a preliminary basis, some simplifications have been chosen to take up to verify the truthfulness or the validity of the assumption at least. For instance, the interface with steel was posited as non-existent as the thermal conductivity of the material is very high, and it follows that the resistance is negligible, given that:

$$R_{steel} = \frac{t_{steel}}{\lambda_{steel}} \leq 1{,}8 * 10^{-4}\ [W\ °C^{-1}]\ , per\ \Delta T > 260℃ \quad \text{(eq.5)}$$

Other formulation for used materials are in Appendix B.

Concerning the method, it should be clarified that the accumulation of energy as a difference of the accumulation initially owned and that transferred, is a result of thermal transmission $Q_i - Q_u$, so:

$$Q_0 - hA\theta = mc_p \frac{d\theta}{d\tau} \quad \text{(eq.6)}$$

This expression is usually resolved by erasing the value of the double integral leading to the more well-known expression:

$$\theta = \theta_i e^{-b\tau}, \begin{cases} \theta = T - T_\infty \\ \theta_i = T_i - T_\infty \end{cases} \quad \text{(eq.7)}$$

Therefore, in the steady-state phase it is observed by data that:

$$\tau_t{}^{-1} = \frac{hA}{\rho V c_p} \propto {}^{b}/_{T} \quad \text{(eq.8)}$$

The problem then shifts to the search for the law of variation of the initial reference temperature as follow. Conversely, the observed initial peak heat loss in each case the supplied energy was suspended, either electrical boiler or solar trough of salt circulation, has also been studied in form of an impulse, but it is not included in this paper. Therefore, the initial temperature has been taken after this first peak phase, Fig. 4 peak area.

Still concerning the method, the behaviour of the salts in the thawing phase due to the temperature natural decay were studied on a different tank during the SFERA III second experimental campaign, so-called Reslag. This tank has a scalable geometry according to (eq. 1) and it was fundamental for the verification and definition of transient temperature response of lumped capacitance for the thermal time constant.

As matter of fact, the possibility to relay on a natural trend of molten salt has led to associate each observable conditions around the tank with a lumped-circuit concept.

In accordance with picture Fig. 3, a multi-switch operates different electrical circuits settled with the action or reaction observed. Hence, Fig. 3 shows the electrical circuit associated to boundary conditions during the natural decay of temperature. The values of capacitor are the molten salt lumped thermal capacitance in Fig. 5, namely the initial cumulated energy at shown stage, while the resistances are convection layer heat loss towards stream like ullage and transient conduction towards solid materials like insulation of tank.

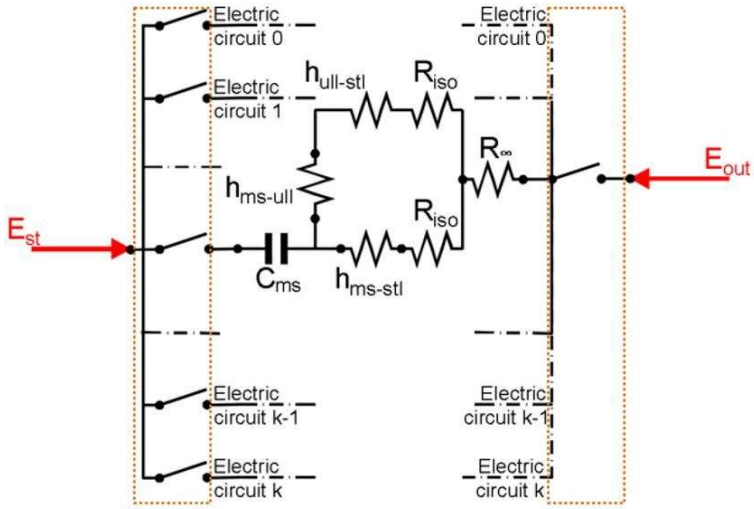

Fig. 3 Lumped-circuit model where each electric circuit corresponds toa group of boundary conditions according to the observed tank case or phase

3. Modelling equations

The novel full-bodied model and its development would require more than one paper according to conditions among most the condition summarized in (eq.16) ; therefore, equation modeling and their boundary conditions are as per the diagram in Fig. 3, postponing in the final outlook some conclusions and further improvements.

As mentioned in Section 2. Methods, the modelling of temperature decay equation starts from a general regression or so-called Newton's non-linear problem. The natural regression of a data cloud strongly depends on how close the initial condition is to have a convergence of the curve. Being more specific, given the temperatures **y** recorded each time interval **t**, the problem can be presented generically as follows (where **x**-es are recorded temperatures):

$$x_{k+1} = x_k - \frac{g(x_k)}{g'(x_k)} \Leftrightarrow g(x_0) = 0 \Longrightarrow \begin{cases} x_{0+1} = x_0 - \frac{g(x_0)}{g'(x_0)} = x_0 \\ x_{1+1} = x_1 - \frac{g(x_1)}{g'(x_1)} \\ \vdots \end{cases} \quad \text{(eq.9)}$$

If we extend the problem to multiple recorded temperatures, in presented tank means 3 thermocouples, it follows that the general expression can be written in vector form as (typical in-use Math notation):

$$x_{n+1} := x_n - \frac{S\prime(\tilde{x})}{S''(\tilde{x})} \Leftrightarrow \begin{cases} S'(\widetilde{x_0}) = 0 \\ \nabla S(\tilde{x}) = S'(\tilde{x}) \\ \boldsymbol{S}''(\tilde{x}) = \begin{bmatrix} \frac{\partial^2 f}{\partial x_1^2} & \frac{\partial^2 f}{\partial x_1 x_2} & \frac{\partial^2 f}{\partial x_1 x_3} \\ \frac{\partial^2 f}{\partial x_2 x_1} & \frac{\partial^2 f}{\partial x_2^2} & \frac{\partial^2 f}{\partial x_2 x_3} \\ \frac{\partial^2 f}{\partial x_3 x_1} & \frac{\partial^2 f}{\partial x_3 x_2} & \frac{\partial^2 f}{\partial x_3^2} \end{bmatrix} \end{cases} \quad \text{(eq.10)}$$

Trivially, the Hessian matrix, thus generically defined, is resolved in the following way, called $\tilde{a}, \tilde{b}$, the regression coefficients of the temperatures recorded in vector form:

$$f(\tilde{a}, \tilde{b}, \tau) = \tilde{a} e^{-\tilde{b}\tau} \quad \text{(eq.11)}$$

Given that:

$$\boldsymbol{S}(\tilde{a}, \tilde{b}) = det \begin{bmatrix} S(\tilde{a}) \\ S(\tilde{b}) \end{bmatrix} = \sum_{i=1}^{n} \left(\tilde{a} e^{-\tilde{b}\tau_i} - T_i\right)^2 \quad \text{(eq.12)}$$

As first approximation, the concerned regression relationship can be considered valid for the temperatures that naturally decay according to the following general equation (eq.13) (Dark dots line in Fig. 4), so:

$$T = T_i e^{-b\tau} \quad \text{(eq.13)}$$

Consequently, eq.9 doesn't give any other change if an action or reaction occurs. As result of the investigation between the natural decay of tank temperatures and the thermal constant of time, it has been developed by complete solution of the differential equation (eq.14). Experimentally, it provides an excellent approximation of the decay of temperature under a set of imposed assumptions, Fig. 4 red line targeted IP.

$$Q_0 - hA\theta = mc_p \frac{d\theta}{d\tau} \quad \text{(eq.14)}$$

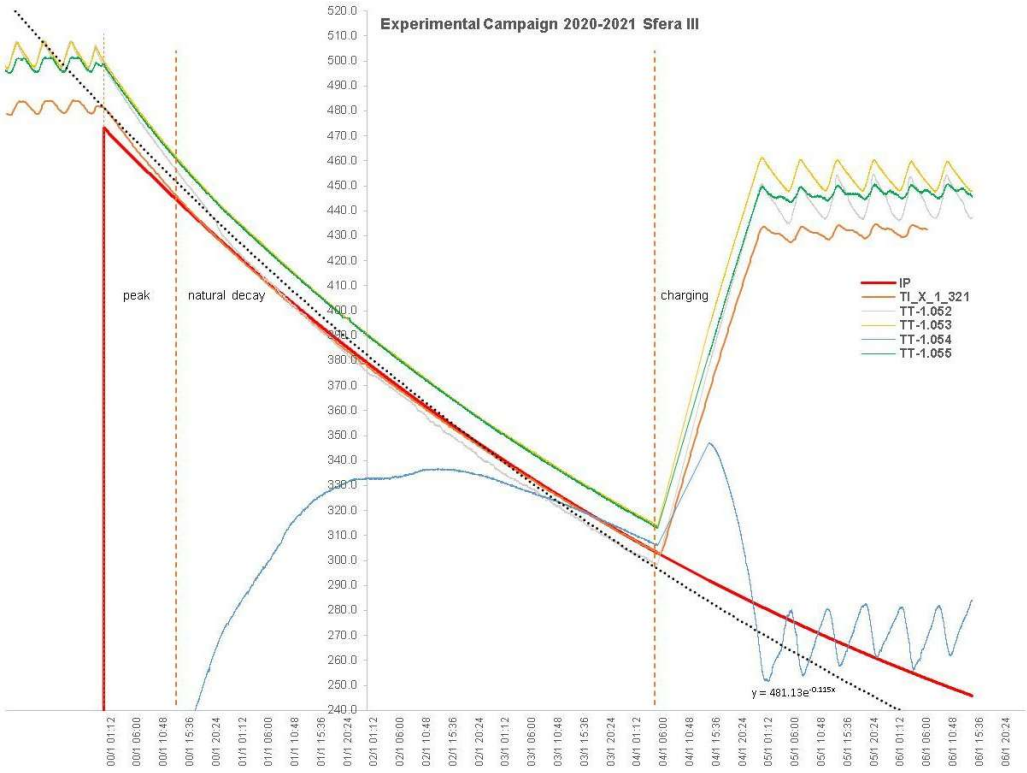

Fig. 4 The orange line shows TIX-1-321 thermocouple of thermocline skin tank along natural temperature decay. The red one is the simulated curve (IP in the chart), and the dark dots line is approximation according to natural regression.

As matter of fact, called Q_0 as the initial stored energy, and defined the thermodynamic parameters according

to exemplified lumped-circuit abstraction in Fig. 5, namely found the equivalent values of the reference electrical circuit, i.e., heat transfer coefficient assumed under the boundary conditions between the interfaces of the materials, and the initial accumulation of the capacitor, it can be written in a general manner by literature that:

$$-\frac{hA}{\rho V c_p}\int_0^{\tau} d\tau = \int_{\theta_i}^{\theta}\frac{d\theta}{\theta} - \frac{Q_0}{\rho V c_p}\int_0^{\tau}\int_{\theta_i}^{\theta}\frac{d\theta}{\theta}d\tau \qquad \text{(eq.15)}$$

The eq.15 could have different solution according to how the initial stored energy varies, and whether an error function should have been applied – known in literature and applications with semi-infinite solid transient heat flow –. These involved mathematical conditions can be listed as below. Here, the paper holds shortly the solution according to the third one among the list in (eq.16).

$$\begin{aligned}
&1-Q_0{=}0 \quad \wedge erf(\eta_a){=}0\\
&2-Q_0{=}const. \wedge erf(\eta_a){=}0\\
&\mathbf{3-\ Q_0{:}Q_0(\tau)\ \wedge\ erf(\eta_a){=}0}\\
&4-Q_0{:}Q_0(\theta)\ \wedge\ erf(\eta_a){=}0\\
&5-Q_0{=}0 \quad \wedge\ erf(\eta_a){\neq}0\\
&6-Q_0{=}const. \wedge erf(\eta_a){\neq}0\\
&7-\ Q_0{:}Q_0(\tau)\ \wedge erf(\eta_a){\neq}0\\
&8-Q_0{:}Q_0(\theta)\ \wedge erf(\eta_a){\neq}0\\
&9-Q_0{:}Q_0(\theta,\tau) \wedge erf(\eta_a){=}0\\
&10-Q_0{:}Q_0(\theta,\tau) \wedge erf(\eta_a){\neq}0
\end{aligned} \qquad \text{(eq.16)}$$

Firstly, the analysis of initial temperature has been observed by the received data, and initial approximations of the differential calculus, named the initial temperature of thermocouple *TT* in the subscript, $T_{i,TT}$, can be trivially obtained as in eq.17, which within a temperature range [260°C,600°C] of molten salts, has a statistical tolerances that can be evaluated as in eq.18 (Please note that temperatures are highly dependent on the place of installation of the tank and the date referred to T_∞).

$$\theta_i = T_i - T_\infty \qquad \text{(eq.17)}$$

$$T_{i,TT} = \underset{bd}{T_{max}}(\pm 5°C) + T_\infty(\pm 7°C) \qquad \text{(eq.18)}$$

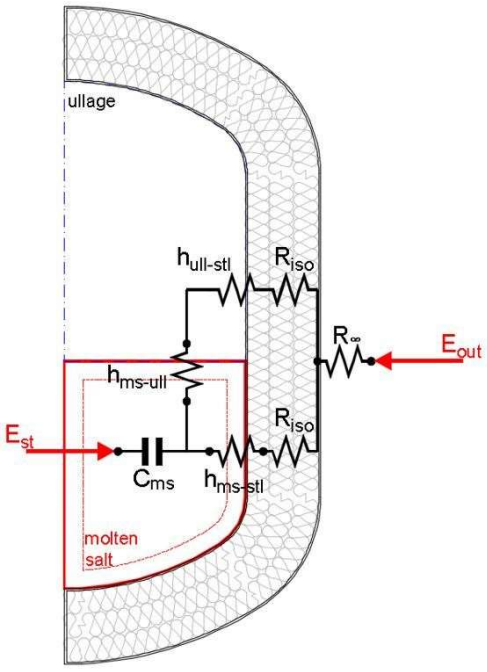

Fig. 5 Lumped-circuit abstraction under a set of imposed assumptions of tank at ENEA Casaccia Roma – Used in this modelling along experimental campaigns and based on data since 2004. The resistance in the pictures are equivalent one according to transient and materials in use (Appendix B).

The same initial temperature is also found trough modelling as a weighted average with respect to the level of molten salts, i.e., its volume in the cooling phase. In fact, it occurs that $T_{i,TT}$ is equal to:

$$T_{i,TT} = T_0(\tau, H_{lms}) + T_\infty \quad \text{(eq.19)}$$

Where $T_0(\tau, H_{lms})$ is the initial temperature weighted as a function of the time intervals in which the salt level and the volume of the salts vary, therefore equal to:

$$T_0(\tau, H_{lms}) = \sum \left(\left(\prod_i \frac{T_{TT,max,i} + T_{TT,min,i}}{2} \frac{V_{ms,i}}{V_T} \right)^{\frac{1}{i}} + \left(\prod_j \frac{T_{TT,max,j} + T_{TT,min,j}}{2} \frac{V_{ull,j}}{V_T} \right)^{\frac{1}{j}} \right)_{,k} \frac{\Delta\tau_k}{\Delta\tau} \quad \text{(eq.20)}$$

Thus, obtaining an expression entirely dependent on physical and geometric parameters. Furthermore, the skin-temperature could be intended as quasi-uniform, but the proportion between the molten salt mass and ullage becomes fundamental to determine this temperature, especially during variations of molten salt level. The existence of outer thermocouples installed on tank-skin aid to find a consistent relationship between inner crossover curves and out crossover curves. This has been explained by Fig. 6, in which the three thermocouples should show the same temperature theoretically, but indeed they behave differently when crossover. In other words, if there is a greater heat loss on a point of the tank and therefore is cooling faster, it is truism consider that the heat flow on an ideal horizontal section is directed towards this area. This calls into question the stability of the temperature of the mass of salts extracted ideally on the horizontal section from a certainly fixed point corresponding to the pump, for instance. Hence, the referred equation (eq.14) according to third boundary conditions in (eq.16) could be written in the form:

$$\frac{d\theta}{d\tau} - \frac{hA}{mc_p}\theta = \frac{1}{mc_p}Q_0 \quad \text{(eq.21)}$$

This is a first order linear differential equation of type:

$$\frac{d\theta}{d\tau} + f\theta = ag \quad \text{(eq.22)}$$

Where the initial accumulated energy is imposed dependent on time $Q_0(\tau) = g(= Q_{0,\tau})$, and the coefficients f and a could be taken as constant in the range of natural temperature decay. So, the solution is known as:

$$\theta = \frac{\int e^{-f\tau} Q_{0,\tau} d\tau + \kappa_0}{e^{-f\tau}} = \frac{\int e^{-f} \ Q_{0,\tau} d\tau + \theta_i e^{-2bf\tau}}{e^{-f\tau}} \quad \text{(eq.23)}$$

The value κ_0 is found out by imposing that this solution could be equal to the condition $Q_0(\tau) = 0$, i.e., not time dependent (Condition 1 in eq.16). As result, the problem became how to find the function $Q_{0,\tau}$. The solution of the equation for temperature decay of molten salt has been figured out by observing that (eq.23) can trivially be written as:

$$\theta_I + \theta_{II} = \frac{\int e^{-f} \ Q_{0,\tau} d\tau}{e^{-f\tau}} + \theta_i e^{-b\tau} \quad \text{(eq.24)}$$

Considering that an error function is set to zero, $erf(\eta_a) = 0$, because it is not the case here, consistently with the sum addenda:

$$\theta_I = \frac{\int e^{-f\tau} Q_{0,\tau} d\tau}{e^{-f\tau}} \quad \text{(eq.25)}$$

Differentiating both members, the result $(1 + f)/(-f) \cong 1$, so:

$$d\theta_I = e^{-f\tau} Q_{0,\tau} d\tau \quad \text{(eq.26)}$$

This could be written as:

$$c(= Q_{0,\tau}) \frac{d\tau}{\tau} = \frac{d\theta_I}{\tau e^{-f\tau}} \quad \text{(eq.27)}$$

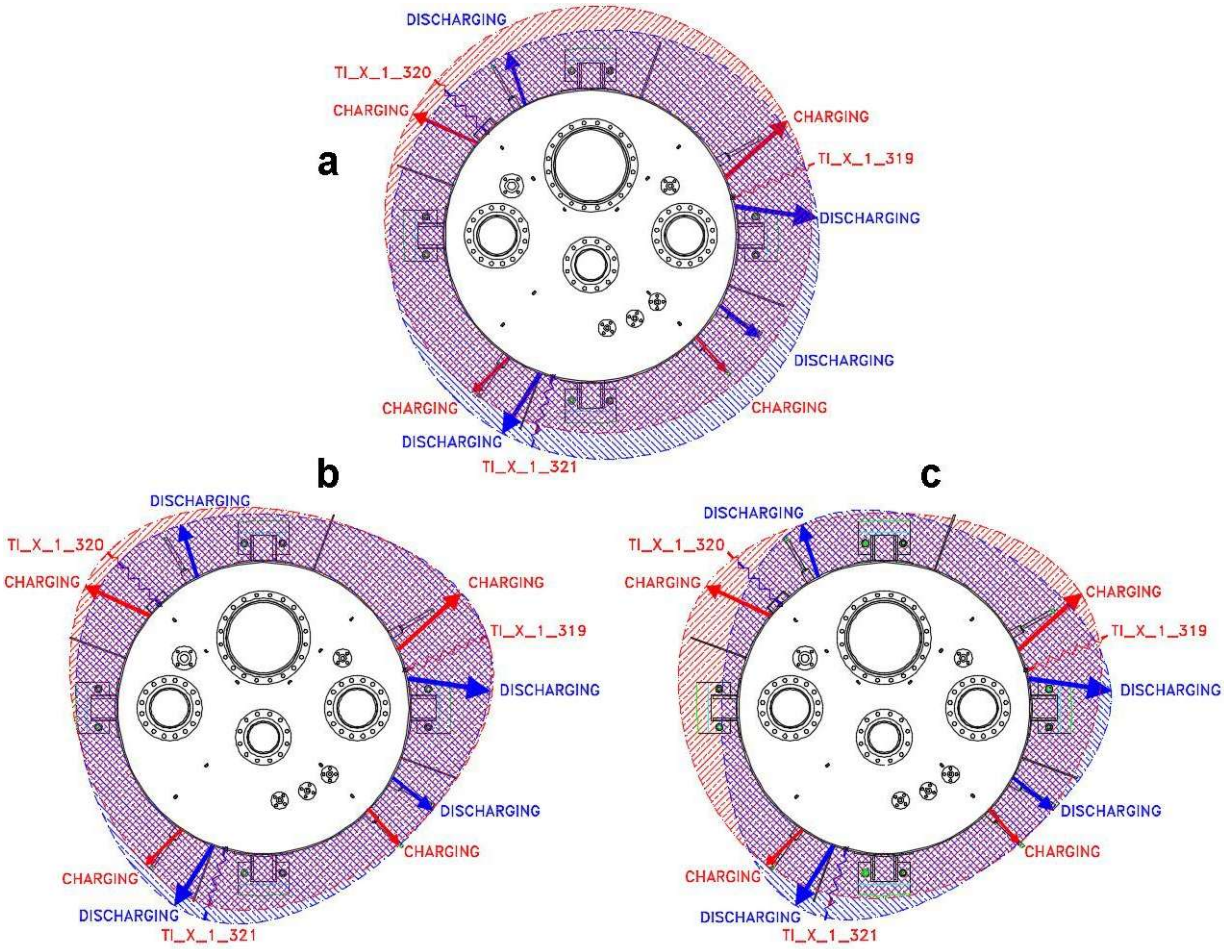

Fig. 6 Blue hatch and dashed lines point the discharging phase, i.e. TIX319>TIX321>TIX320, while red hatch and dashed lines point the charging phase, i.e., TIX319>TIX320>TIX321. The shapes are weightings between the 3external and internal temperatures by thermocouples at different angles

The second member are temperatures over time, therefore can be re-written compactly:

$$c = \frac{\int \frac{d\theta^*}{\theta^*}}{\int \frac{d\tau}{\tau}} \qquad \text{(eq.28)}$$

By integrating and applying the properties of the logarithms of the base change, the result is:

$$c = \frac{\ln(\theta^*(\tau))}{\ln(\tau)} \Rightarrow c = \log_\tau \theta^* \qquad \text{(eq.29)}$$

To conclude, the searched equation is:

$$\theta = \theta_i e^{-b\tau} + \tau^c \qquad \text{(eq.30)}$$

This equation can simulate the natural temperature decay accurately – Fig. 4 targeted IP –.

Finally, this new application with lumped-capacitance circuit in Fig. 5 and the third conditions in eq.16 leads to solution in (eq.30). The value sought with respect to b as a function of the time constant τ_t given the probability of error based on a standard deviation σ has been omitted to focus on the presented result in Fig. 4 which is similar to any other thermocouple at the same conditions. This is extremely interesting because of able to simulate what happen accurately around and inside the tank. However, during the experimental phase, the temperatures θ are measured, and correspond to the trend from the tank-storage setpoint to the minimum temperature set (300°C in Fig. 4). Conversely, during the design phase the temperature design will be the compensation of average outdoor temperature in free stream condition that allows to find the coefficient b,

namely it depends on the time constant given a scheme in Fig. 5 with significant advantages concerning on-design performing solutions. To be consistent the search of this value has been postponed to an ongoing further project-work being strictly connected to the chosen both boundary conditions and the lumped circuit.

4. Conclusion and outlook

From the experimental data to the modelling and improving of a governing equation, which uses an initial thermal stored energy varying on time, it can be drawn an advantage in terms of obtained more understanding of heat loss, but also, the lowering temperatures of the salts as a function of internal physical parameters. This investigative analysis allows to simulate accurately the trend of the temperatures inside the tank volume in the operation conditions concerning point 3 at (eq.16), i.e., natural temperature decay, which will have some relationship with discharging ones. Indeed, the discharging operation is essential for the thermal energy demand. Hence, to analyze how the molten salt behaves in several boundary conditions according to the applied lumped capacitance concept in dynamic mode, grant the right temperature to the power block. Closely related to the results of this paper, the heat transfer equation can be solved in a non-trivial way, not neglecting the fact that the initial energy of a system is not zero, and that its temperature decays in relation to time, where no other specific condition occurs. The novelty is limited to the presented conditions along the paper. However, proceeding is essential to build up a correct aid for sizing and make right geometry for storages, or any tank prone to be a thermal storage, especially thermocline one. Therefore, further improvement and an outlook of reliable developments, which are already ongoing, are worth to be mentioned:

- completing all assumptions as starting point for evidence
- discretization and simulation of model
- validation based on experimental data
- on-design tank modelling
- off-design tank modelling

Acknowledgement

We thank ENEA for the support of its scientific and technical staff provided during the access SURPF2001170003A to PCS facility. The access SURPF2001170003A was arranged in the frame of H2020 SFERA-III project activities – European Union's Horizon 2020 G.A. n. 823802 –.

Reference

T. L. Bergman, A. S. Lavine, 2017, Fundamentals of heat and mass transfer, Wiley, 8th edition.

Chao Xu, Zhifeng Wang, Yaling He, Xin Li, Fengwu Bai, 2012, Parametric study and standby behavior of a packed-bed molten salt thermocline thermal storage system, Renewable Energy, 48 , 1–9

Chau Xu, Zhifeng Wang, Yaling He, Xin Li, Fengwu Bai, 2012, Sensitivity analysis of the numerical study on the thermal performance of a packed-bed molten salt thermocline thermal storage system, Applied Energy, 92, 65–75

W. Gaggioli, F. Fabrizi, L. Rinaldi, P. Di Ascenzi, 2017, Experimental tests about the cooling/freezing of the molten salts in the receiver tubes of a solar power plant with parabolic trough conditions, AIP Conference Proceedings 1850, 020005.

W. Gaggioli, L. Rinaldi, P. Tarquini, 2018, Thermal characterization of a stratifying molten salts storage tank with integrated steam generator in real operating conditions, AIP Conference Proceedings 2033, 070011.

S.V. Garimella, S.M. Flueckiger, 2012, Second-law analysis of molten-salt thermal energy storage in thermoclines, Solar Energy, 86, 1621-1631

D.W. Green, R. H. Perry, 2008, Perry's Chemical Engineers' Handbook, Wiley, 8th edition.

J.E. Pacheco, S.K. Showalter, W.J. Kolb, 2002, Development of molten-salt thermocline thermal storage

system for parabolic trough plants, Journal of Solar Energy Engineering, 124(2), 153-159.

C. Turchi, D. Bharathan, G. Glatzmaier, M. Wagner, C. Libby, L. Cerezo, R. Bedilion, Solar Thermocline Storage Systems: Preliminary Design Study, 2010, EPRI, Palo Alto, CA: 1019581.

A. B. Zavoico, 2001, Solar power tower design basis document. Sandia National Laboratories. Report no. SAND2001-2100.

Appendix A

Tab. 1 ENEA experimental data, received and analyzed, in accordance with the PCS operating conditions ongoing recorded – Log registration in column ENEA LOG-RECORDS Yes=1 means existence and studied data accordingly, No=0 (only data) means it was not possible to get the log registration in that day or period or day for several reasons.

Prg.	Date in: 2004 2005 2008	ENEA LOG-RECORDS Yes=1 No=0 (only data)	Prg.	Date in: 2008 2018 *2020-2021 SFERA III*	ENEA LOG-RECORDS Yes=1 No=0 (only data)
1	02.04.2004	1	23	01.04.2008	1
2	05.04 to 08.04.2004	1	24	09.07.2008	1
3	09.04 to 12.04.2004	0	25	17.09.2008	1
4	13.04 to 16.04.2004	1	26	25.09.2008	1
5	17.04 to 19.04.2004	0	27	01.10.2008	1
6	20.04 to 21.04.2004	1	28	08.10.2008	1
7	26.04 to 30.04.2004	1	29	16.12.2008	1
8	01.05 to 02.05.2004	0	30	22.12.2008	1
9	07.05.2004	1	31	27.08 to 30.08.2018	0
10	14.05.2004	1	32	05.09 to 06.09.2018	0
11	17.05.2004	0	33	17.09 to 18.09.2018	0
12	18.05.2004	1	34	18.10 to 22.10.2020	0
13	19.05.2004	0	35	02.02 to 04.02.2021	0
14	20.05 to 22.05.2004	1	36	20.07 to 24.08.2021	0
15	25.06 to 23.08.2004	0	Miss a period test for power loss along CSP because of service		
16	24.08 to 27.08.2004	1			
17	28.08 to 29.08.2004	0			
18	30.08 to 31.08.2004	1			
19	01.09 to 17.09.2004	1			
20	14.01 to 18.01.2005	0			
21	28.02.2008	1			
22	12.03.2008	1			

Appendix B

Tab. 2 Thermal-physical properties and constitutive correlation to the temperature

Material	Thermal physical property	Equation
Air, *air = ull*	Thermal conductivity, k_{air}	$k_{air} = 0{,}224 + (8{,}02)10^{-4}\,T - (3{,}28)10^{-7}\,T^2 [W\,m^{-1}\,°C^{-1}]$
	Density, ρ_{air}	$\rho_{air} = 2{,}8953 + 0{,}26733\,T + 132{,}45\,T^2 + 0{,}27341\,T^3 [K]\ [kg\,m^{-3}]$
	Specific heat, $c_{p,air}$	$c_{p,air} = 0{,}10 + (1{,}40)10^{-4}\,T + (1{,}01)10^{-7}\,T^2 - (5{,}69)\,10^{-11}\,T^3\ [J\,kg^{-1}°C^{-1}]$
	Viscosity, μ_{air}	$\mu_{air} = [0{,}1726 + (4{,}52)10^{-4}\ T - (1{,}937)10^{-7}\,T^2 + (4{,}185)10^{-11}\,T^3]\,10^{-4}\ [°C]\ [kg\,m^{-1}s^{-1}]$
Stone mineral wool, *iso*	Thermal conductivity, k_{iso}	$k_{iso} = 0{,}106\ [W\,m^{-1}\,K^{-1}]$
	Density, ρ_{iso}	$\rho_{iso} = 100[kg\,m^{-3}]$
	Specific heat, $c_{p,iso}$	$c_{p,iso} = 1030\ [J\,kg^{-1}K^{-1}]$
Molten salt, *ms*	Thermal conductivity, k_{ms}	$k_{ms} = 0{,}443 + 1{,}9 \times 10^{-4}\,T\ [W\,m^{-1}\,°C^{-1}]$
	Density, ρ_{ms}	$\rho_{ms} = 2090 - 0{,}636\,T[°C]\ [kg\,m^{-3}]$
	Specific heat, $c_{p,ms}$	$c_{p,ms} = 1443 - 0{,}172\,T\ [J\,kg^{-1}°C^{-1}]$
	Viscosity, μ_{ms}	$\mu_{ms} = [22{,}714 - 0{,}12\,T + 2{,}281 \times 10^{-4}\,T^2 - 1{,}474\ \times 10^{-7}\,T^3]\ \times 10^{-3}[°C]\ [kg\,m^{-1}s^{-1}]$
Steel, *stl*	Thermal conductivity, k_{stl}	$k_{ms} = 60\ [W\,m^{-1}\,K^{-1}]$
	Density, ρ_{ms}	$\rho_{stl} = 8000[kg\,m^{-3}]$
	Specific heat, $c_{p,stl}$	$c_{p,stl} = 480\ [J\,kg^{-1}K^{-1}]$
Aluminum, *alu*	Hemispherical emissivity	$\varepsilon = 0{,}1\ [-]$